

Petrology of explosive Middle-Upper Triassic ultramafic rocks in the Mess Creek area, northern Stikine terrane



D. Milidragovic^{1, a}, N.L. Joyce², A. Zagorevski², and J.B. Chapman¹

¹ Geological Survey of Canada, 1500-605 Robson Street, Vancouver, BC, V6B 5J3

² Geological Survey of Canada, 601 Booth Street, Ottawa, ON, K1A 0E8

^a corresponding author: Dejan.Milidragovic@canada.ca

Recommended citation: Milidragovic, D., Joyce, N.L., Zagorevski, A., and Chapman, J.B., 2016. Petrology of explosive Middle-Upper Triassic ultramafic rocks in the Mess Creek area, northern Stikine terrane. In: Geological Fieldwork 2015, British Columbia Ministry of Energy and Mines, British Columbia Geological Survey Paper 2016-1, pp. 95-111.

Abstract

The Mess Lake facies of the Stuhini Group (Middle to Upper Triassic) in northwestern British Columbia includes a unit of pervasively serpentinized, olivine-rich, subaqueous lapilli breccia, lapilli tuff, and ash tuff. Relatively high whole-rock MgO concentrations (29-38 wt.%; loss on ignition-free) of pyroclastic samples from this unit reflect significant accumulation of olivine. These ultramafic pyroclastic rocks also exhibit strong enrichment in Ba and depletion in Nb+Ta relative to La, consistent with derivation from slab-metasomatized mantle asthenosphere in a volcanic arc setting. The restored parental liquid is a primitive, mantle-derived, arc magma that contained up to 16-20 wt.% MgO. The unit contains fresh volcanic glass indicating low-grade regional metamorphism, and suggesting that it postdates emplacement of the nearby Hickman pluton, which yielded ⁴⁰Ar/³⁹Ar hornblende ages of 222.2 ±2.8 Ma, 221.6 ±2.5 Ma, and 220.1 ±2.7 Ma. The Alaskan-type ultramafic plutons of the Polaris suite (Middle to Late Triassic) and a post-Hickman basaltic diatreme, containing picritic fragments, are spatially associated and broadly coeval with the ultramafic pyroclastic rocks of the Mess Lake facies, but a petrogenetic link has yet to be established.

Keywords: Stuhini Group, Triassic, pyroclastic, ultramafic, Stikinia

1. Introduction

The Stikine terrane (Stikinia) of the Canadian Cordillera (Fig. 1) is a Mesozoic volcanic arc (see Nelson et al., 2013 for recent overview) that hosts over 1000 Cu ±Au-Mo-Ag porphyry occurrences (British Columbia Geological Survey, 2015; Yukon Geological Survey, 2015). Logan and Mihalynuk (2014) estimated that ≥90% of the Cu mineralization in the Stikine and adjacent Quesnel terrane to the east formed during a relatively short-lived (~6 m.y.) mineralizing epoch centred at ~205 Ma, which spans the Triassic-Jurassic boundary. This episode of porphyry mineralization has been attributed to a thermal spike in the underlying mantle wedge that resulted in mobilization of hydrous, metal-rich fluids. Logan and Mihalynuk (2014) attributed the elevated geothermal gradient to arc-parallel tearing of the Panthalassan oceanic plate as it subducted beneath Stikinia at ~210 Ma, based on the appearance of rare, strongly alkaline lavas and ultramafic (picritic) rocks. In the Mess Lake area, ~130 km southwest of the town of Dease Lake, ultramafic olivine-rich pyroclastic tuff forms the base of the Mess Lake volcanic facies (Logan et al., 2000) of the Stuhini Group (Middle to Upper Triassic), mainly along the eastern margin of the Hickman pluton (Fig. 2). Possibly related to these pyroclastic rocks are the broadly coeval, spatially associated ultramafic intrusions of the Polaris suite (Middle to Late Triassic; Nixon et al., 1989; Logan and Koyanagi, 1994; Brown et al., 1996), which border the Hickman pluton. Establishing a genetic and temporal relationship between the Middle to Late Triassic ultramafic rocks would add further credence to the

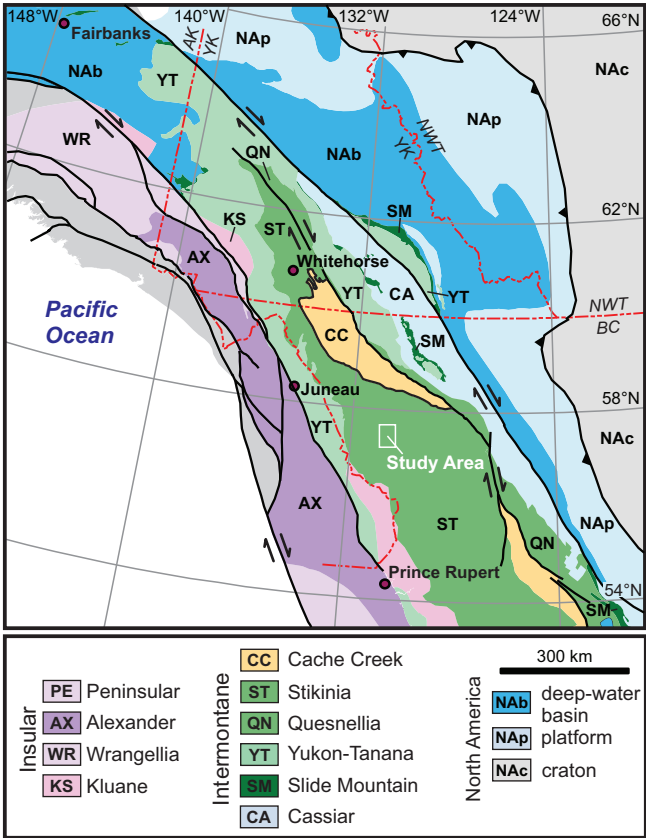


Fig. 1. Terrane map of the northern Canadian Cordillera showing the location of the study area (modified from Nelson et al., 2013).

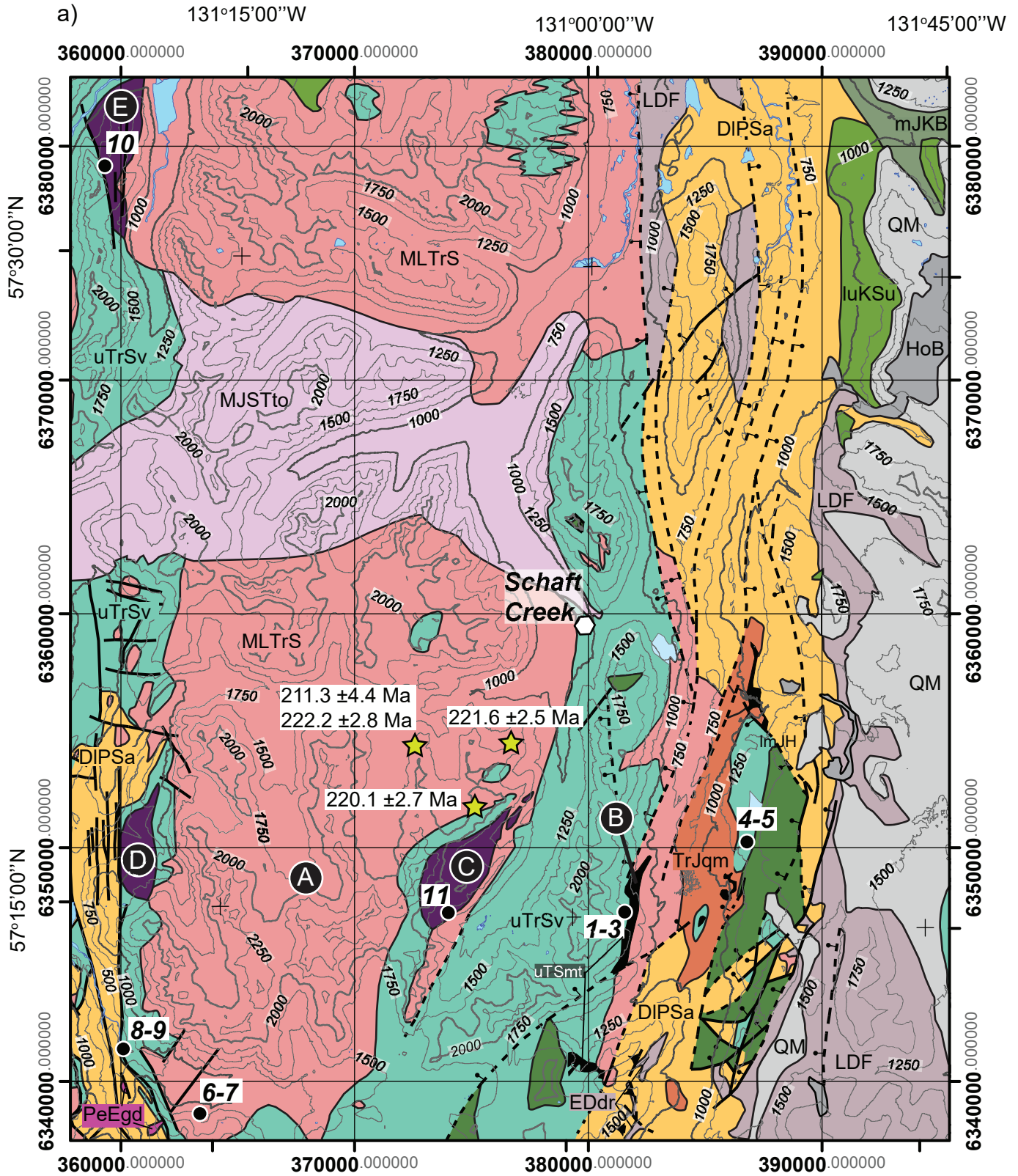
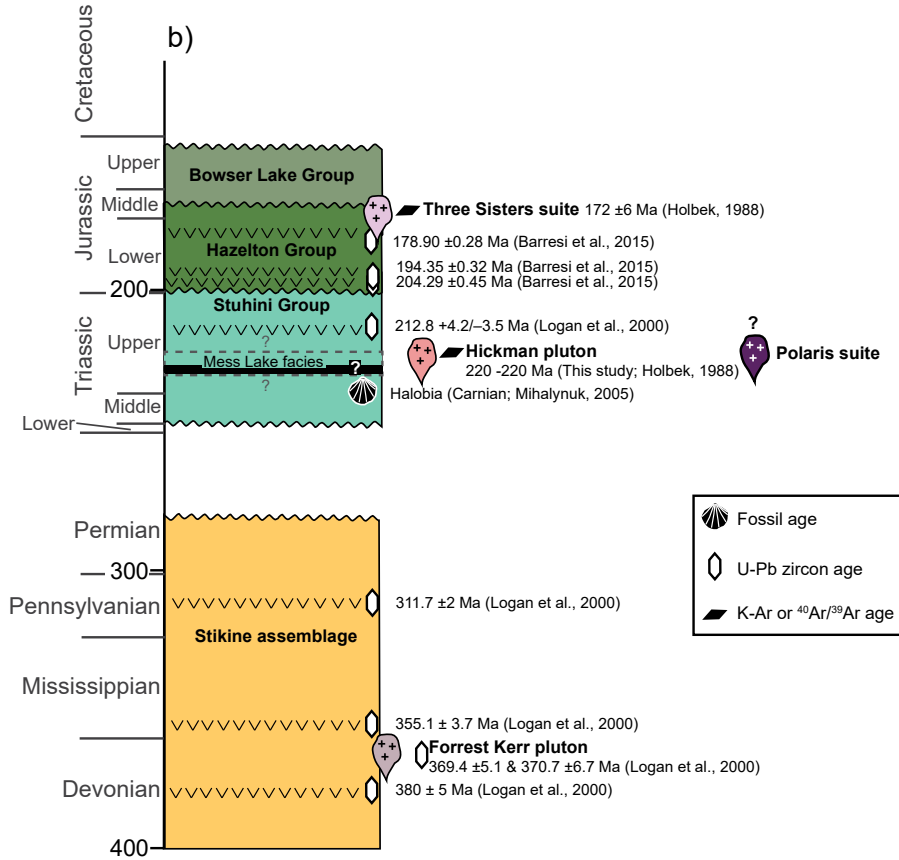


Fig. 2. a) Simplified geological map of the Mess Lake area (parts of NTS 104G 02, 03, 06, 07, 10, and 11; modified from Logan et al., 2000 and Mihalyuk et al., 1996), showing the Schaft Creek exploration camp and locations of samples analyzed for geochemistry (1-11; Table 2) and $^{40}\text{Ar}/^{39}\text{Ar}$ geochronology (yellow stars). Key locations discussed in the paper are labeled A-E. b) Schematic stratigraphic column illustrating the relationships between stratigraphic and intrusive units in the study area.



Legend

INTRUSIVE

Paleocene to Eocene

PeEgd biotite, sphene +/- hornblende granodiorite

Middle Jurassic

MJTSto 3 Sisters suite - tonalite

Late Triassic to Early Jurassic

TrJqm Loon Lake stock - quartz monzonite

Middle Triassic to Late Triassic

MLTrS Stikine suite - Hornblende, (+/- pyroxene)-quartz diorite to granodiorite, tonalite, polyphase leucogabbro and diorite

MLTrP Polaris suite - dunite, olivine pyroxenite, gabbro

Late Devonian

LDF Forest Kerr suite - biotite granite to tonalite

Early Devonian

EDdr Foliated to equigranular green chloritic pyroxene diorite

STRATIFIED

Holocene

HoB Big Raven Formation - Alkaline olivine basalt and Hawaiite

Miocene to Holocene

QM Mount Edziza Complex - trachyte to alkaline olivine basalt and hawaiite; flows and breccias

Lower to Upper Cretaceous

luKSu Sustut Group - chert-pebble conglomerate, quartz sandstone, siltstone, and carbonaceous shale

Middle Jurassic to Middle Cretaceous

mJKB Bowser Lake Group - greywacke, shale, local chert-pebble conglomerate and granule conglomerate lenses

Lower Jurassic to Middle Jurassic

lmJH Hazelton Group - Marine epiclastic and volcanic, and coarse clastic (conglomerate, grit, greywacke) rocks

Middle to Upper Triassic

uTrSv Stuhini Group - Mess Lake facies - mafic to intermediate lapilli tuff, lesser ash, breccia & tuffite. Green and maroon, massive plagioclase and/or augite-phyric basaltic flows, sills and dykes. Epiclastic sandstone interbedded with conglomerate

uTSmt Greyish-brown to green-weathering olivine lapilli and ash tuff

Devonian to Lower Permian

DIPSa Stikine assemblage - foliated Paleozoic volcanic, clastic, and carbonate rocks

KEY UNITS

A Hickman pluton - Stikine suite

B Mess Lake facies ultramafic tuff (Fig. 3)

C Mt. Hickman ultramafic complex - Polaris suite

D Middle Scud ultramafite - Polaris suite

E Yehiniko ultramafite - Mess Creek facies ultramafic tuff

4-5

● Location of samples collected between 2009 -2011 (see table 1 for UTM coordinates and geochemical data)

★ ⁴⁰Ar/³⁹Ar dating site

0 5 10 15

Kilometres

Universal Transverse Mercator grid zone 9
NAD 1983 datum
Contour interval = 250 m

catastrophic events in the sub-arc mantle proposed by Logan and Mihalynuk (2014).

Primitive basaltic liquids (MgO >10 wt.%), derived from the Earth's mantle are important carriers of base (e.g., Ni, Cr) and precious (e.g. platinum group element, PGE) metals into the crust, but depending on the fertility, oxidation state, and volatile content of their source regions, primitive basalts may also be important carriers of Cu, Mo, and Au (Richards, 2015). Furthermore, primitive basaltic liquids and their crustal derivatives provide key information about mantle geodynamics and tectonic setting (e.g., Pearce, 2008). Although mafic and ultramafic rocks offer important constraints on the Late Triassic tectonic and metallogenic evolution of Stikinia and seem to be of regional extent, they remain poorly studied. To better understand Late Triassic mantle-sourced magmatism, we examined ultramafic outcrops in the Mess Lake area (Fig. 2) to document field relationships of ultramafic rocks in the Stuhini Group and the Polaris suite, and to collect a representative suite of samples for further petrographic, geochemical, isotopic and geochronological studies. Herein we integrate petrographic and outcrop-scale observations with geochemical data from 11 samples collected during previous reconnaissance sampling. We also present new $^{40}\text{Ar}/^{39}\text{Ar}$ hornblende ages from four gabbroic to granodioritic samples from the Hickman pluton. We conclude that the ultramafic rocks formed from mantle-derived, primitive arc magmas that likely erupted after ~222 to 220 Ma, when the Hickman pluton was emplaced.

2. Geological background

The Stikine terrane is a composite volcanic arc comprising Devonian to Jurassic volcanic and sedimentary assemblages that are cut by coeval plutonic rocks. Paleozoic rocks of the Stikine assemblage (Monger, 1977) record the first of three episodes of island-arc formation. The second and third episodes are represented by two unconformity-bounded Middle Triassic-Lower Jurassic successions: 1) the Stuhini Group (Middle-Upper Triassic), which consists predominantly of subaqueous, mafic to felsic volcanic and related sedimentary rocks; and 2) the Hazelton Group (Lower-Middle Jurassic) comprising subaqueous to subaerial, volcano-sedimentary rocks (Brown et al., 1996; Logan et al., 2000; Barresi et al., 2015). The Stuhini Group contains voluminous augite and/or plagioclase porphyritic basalt and andesite that are coeval with Carnian to Rhaetian sedimentary rocks (Souther, 1977; Logan et al., 2000; Mihalynuk et al., 1999; Logan and Iverson, 2013). Logan et al. (2000) reported that aplitic dikes extend outward from a hornblende biotite granodiorite to quartz monzonite intrusion on the east-facing slope above Mess Creek and cut the Mess Lake facies of the Stuhini Group. They correlated this plutonic body with the main phase of the Hickman pluton (~221 Ma; Holbek, 1988; this study), implying that the Mess Lake facies is older than ~221 Ma, which may be at odds with our results (see Discussion). The end of Triassic arc building and Stuhini Group deposition is marked by termination of magmatism, deposition of Late Norian to Rhaetian limestones (Sinwa

Formation), and deformation.

Plutonic suites coeval with arc volcanism include Forrester Kerr (Late Devonian), More Creek (Early Mississippian), Stikine, Polaris, and Copper Mountain (Late Triassic), Texas Creek, Aishihik, and Long Lake (Early Jurassic), and Three Sisters (Middle Jurassic; Logan et al., 2000; Zagorevski et al., 2014). The Hickman pluton in the eastern half of the study area (Fig. 2) is a composite intrusion and part of the Stikine Suite (Brown et al., 1996; Logan et al., 2000).

2.1. Late Triassic ultramafic magmatism

The Stuhini Group consists mainly of basaltic to andesitic volcanic rocks that are accompanied by rare felsic volcanic rocks. Ultramafic volcanic rocks are volumetrically minor, but seem to be distributed throughout northwestern Stikinia, including the Mess Lake, Telegraph Creek, Endeavour Mountain, and Atlin Lake areas (Brown et al., 1996; Mihalynuk et al., 1999; Logan et al. 2000). In the Mess Creek area, ultramafic volcanic rocks of the Mess Lake facies unconformably overlie Permian Stikine assemblage limestone and are overlain by massive plagioclase-phyric basalts, massive to weakly stratified mafic tuffs, and plagioclase + augite-phyric basaltic andesite.

In addition to these ultramafic pyroclastic deposits, ultramafic plutonic rocks of the Polaris suite, described as Alaskan-type intrusions by Nixon et al. (1989), also occur along the margins of the Hickman batholith (Fig. 2). These ultramafic intrusions comprise chromite-bearing serpentinized dunite and clinopyroxenite (\pm olivine), and include the Hickman ultramafic complex and Middle Scud ultramafite (Nixon et al., 1989; Brown et al., 1996). Brown et al. (1996) reported a third ultramafic pluton on the western side of the batholith, named the Yehiniko ultramafite.

2.1.1. Ultramafic tuff of the Stuhini Group

The Stuhini Group ultramafic pyroclastic rocks are well exposed ~12 km south-southeast of the Schaft Creek camp (Fig. 2), where they form a 3-5 km long semi-continuous unit that is \leq 100 m thick. Although the ultramafic rocks appear to have served as a locus for late brittle faulting and veining, thick sections are relatively undisturbed. One sub-vertical cliff face exposes a section ~35 m thick (Fig. 3a), cut by a thin (<1 m) hornblende-phyric basaltic dike with chilled margins (Fig. 3b). The outcrop exposes four fining-upward sequences, in which beds, normally graded from tuff breccia to olivine lapilli tuff, are capped by units of rhythmically stratified ash tuff (Figs. 3-5). Each fining-upward sequence has a sharp base, locally marked by low-amplitude scouring of underlying ash tuff, and may record a separate eruption event. The contact between fine lapilli tuff and overlying rhythmically-stratified ash tuff is gradational in all cases. The bomb and lapilli-sized fragments contain abundant black-weathering, euhedral to subhedral, serpentine-after-olivine pseudomorphs and have cusped to embayed margins (Fig. 4a), suggesting minimal deformation during and since deposition. Lapilli are typically vesicular although, in some cases, the internal vesicular microstructure

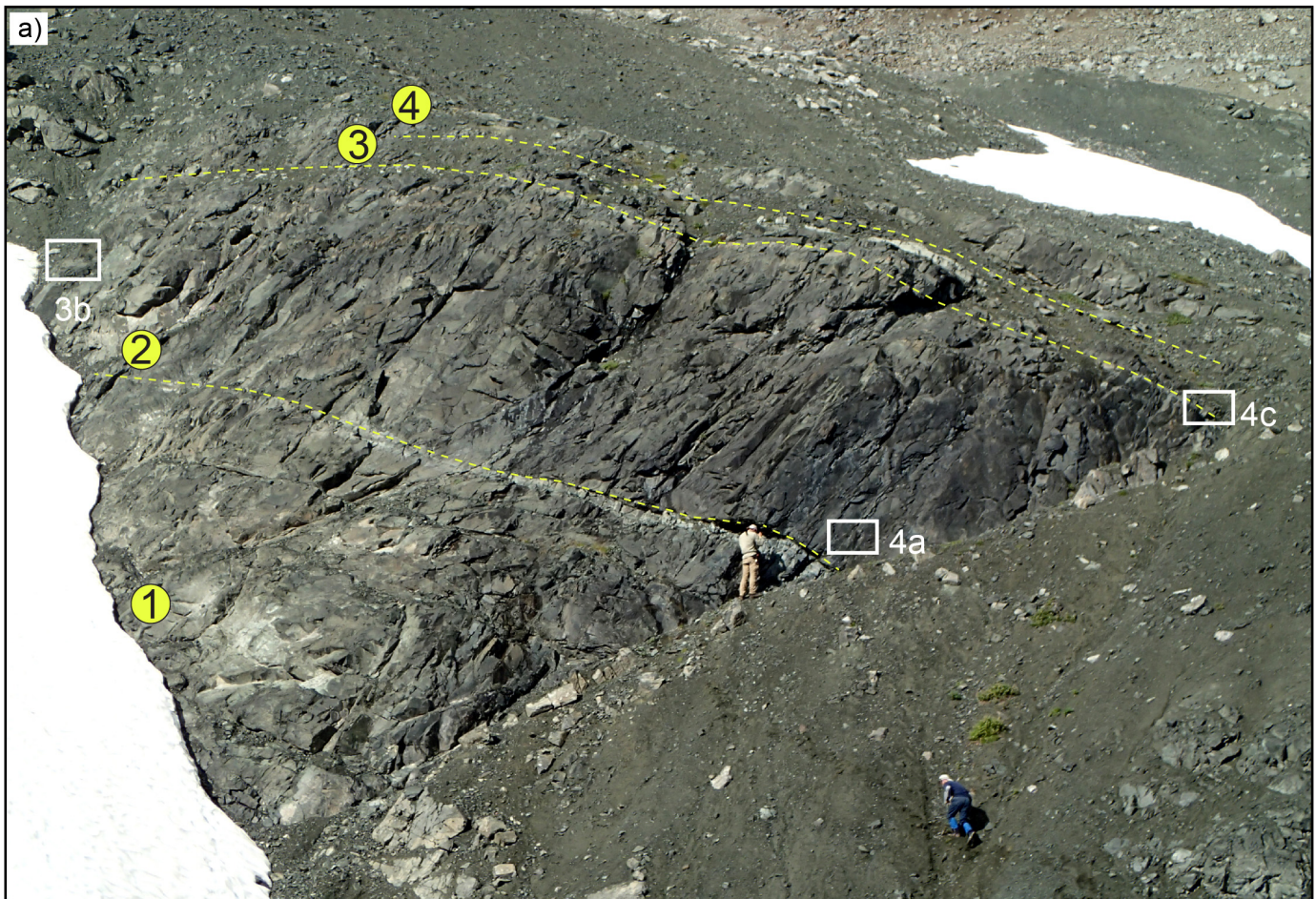


Fig. 3. a) Ultramafic tuffs exposed on a sub-vertical cliff on the west side of the Mess Creek valley, south-southeast of the Schaft Creek exploration camp arranged in four fining-upward sequences (1-4) that follow the order sharp-based tuff breccia to lapilli tuff to ash tuff. White boxes show the positions of Figs. 3b, 4a and 4c. **b)** Hornblende-phyric basaltic dike that cuts pyroclastic rocks on the cliff face in 3a. The size and abundance of hornblende phenocrysts decrease symmetrically from the dike centre.

has been obliterated by devitrification and secondary mineral growth. Some lapilli contain unaltered glass (Fig. 4b), consistent with rapid quenching. The ash tuff is finely to coarsely layered

(≤ 3 mm to ≥ 5 cm), with individual layers that are continuous and parallel at outcrop scale (Fig. 4c). As observed in thin section, this macroscopic layering is the manifestation of gradational variation in the abundance of partially palagonitized glass shards relative to fragmented serpentinized olivine.

Logan et al. (2000) described the Stuhini Group ultramafic rocks as largely altered to serpentine, chlorite and talc. Most lapilli consist of olivine, pseudomorphed by serpentine \pm magnetite and calcite (Fig. 6) in a fine-grained brown groundmass of chlorite, sericite, and other clay minerals; the lapilli float in a matrix of serpentinized olivine, devitrified ash, and chlorite. Less commonly, lapilli are composed entirely of vesicular palagonitized glass (scoria; Fig. 6e). Clinopyroxene is sparse, as are clasts of non-cognate lithologies. Despite pervasive alteration, most ash tuff samples contain bubble-wall shards of partially palagonitized to fresh glass (Fig. 6b).

Brown et al. (1996) mapped ultramafic cumulate rocks at the margin in the Hickman batholith in the Telegraph Creek area, in the northwestern corner of the study area (Yehiniko ultramafite; Fig. 2). Reconnaissance sampling in 2010 indicated that some of these rocks are ultramafic lapilli tuff rather than intrusive rocks. Detailed investigation of the Yehiniko ultramafic body, conducted during this study, revealed abundant ultramafic pyroclastic rocks with ubiquitous, relict olivine (Fig. 6f). Brown et al. (1996) also described other occurrences of Upper

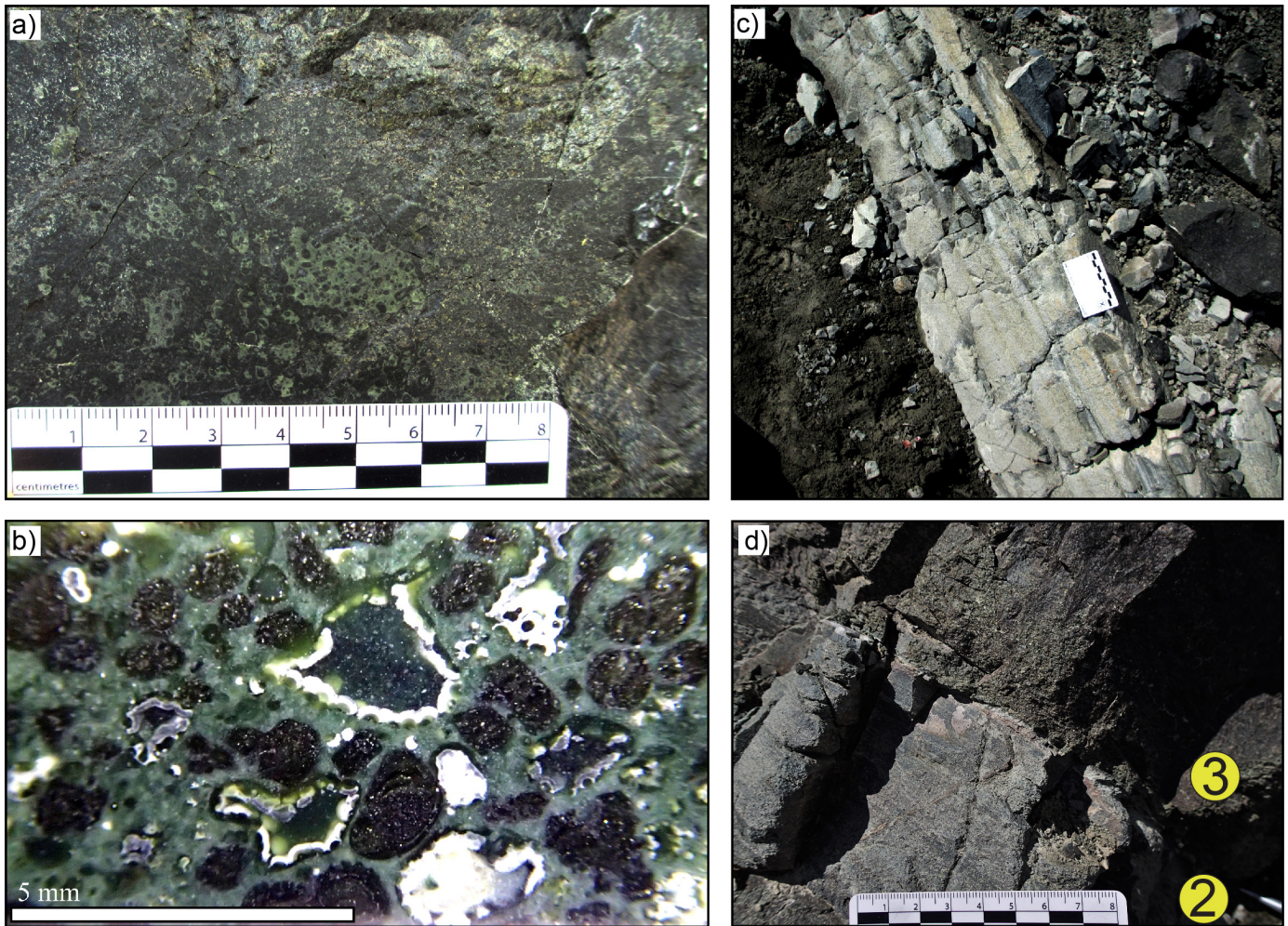


Fig. 4. **a)** Lapilli tuff near the base of fining-upward sequence 2 (Fig 3). A ~2 cm lapilli, containing subhedral olivine (black) in fine-grained, green matrix is in the centre of the photo. **b)** Close-up of a ~3 cm lapillus. The subhedral black crystals are olivine. The cusped, green, vitreous features with white rims appear to be fresh volcanic glass. **c)** Thin rhythmic layering in ash tuff at the top of fining-upward sequence 2. **d)** Abrupt contact between lapilli tuff at the base of fining-upward sequence 3 and underlying ash tuff of fining-upward sequence 2.

Triassic or older ultramafic volcanic rocks in the Endeavour Mountain area, ~30 km east-northeast of Schaft Creek (Fig. 2), supporting the idea of widespread ultramafic volcanism in northwestern Stikinia.

2.1.2. The Hickman pluton

The Hickman pluton of the Stikine suite consists mainly of massive to weakly-foliated, medium grained, equigranular, hornblende biotite granodiorite to quartz monzonite with subordinate tonalite and quartz diorite (Brown et al., 1996; Logan et al., 2000). The pluton also contains gabbroic and dioritic phases. Potassium-argon and Rb-Sr geochronology on biotite and hornblende suggests a minimum emplacement age of ~221 Ma for the Hickman pluton (Holbek, 1988; Brown et al., 1996). At the Schaft Creek deposit, quartz and feldspar-porphyrific apophyses of the Hickman pluton, with a U-Pb zircon age of 220 +15/-2 Ma (Logan et al., 2000) cut Stuhini Group country rocks and are associated with mineralization. At its southern limit of exposure, the Hickman pluton is cut by a

mafic diatreme breccia of unknown age. The breccia consists of cm- to dm- sized hydrothermally altered granitoid and mafic volcanic clasts in a fine-grained plagioclase-phyric basaltic matrix. The mafic volcanic population includes fragments of augite and olivine (now largely chlorite)-phyric basalt/picrite, which we sampled due to its primitive mineralogy and composition, and possible genetic ties to ultramafic rocks of the Mess Lake facies and/or Polaris suite.

2.1.3. Ultramafic cumulate rocks of the Polaris suite

Evaluating the possibility of a genetic relationship between the Middle to Late Triassic ultramafic intrusions of the Polaris suite (Nixon et al., 1989; Brown et al., 1996) and the ultramafic pyroclastic rocks of the Stuhini Group is important for understanding the extent, timing and duration of the Middle to Late Triassic magmatism in northwestern Stikinia. The Mount Hickman ultramafic complex, on the southeastern margin of the Hickman pluton (Fig. 2), consists mainly of olivine-clinopyroxenite and gabbro; serpentinized dunite is locally

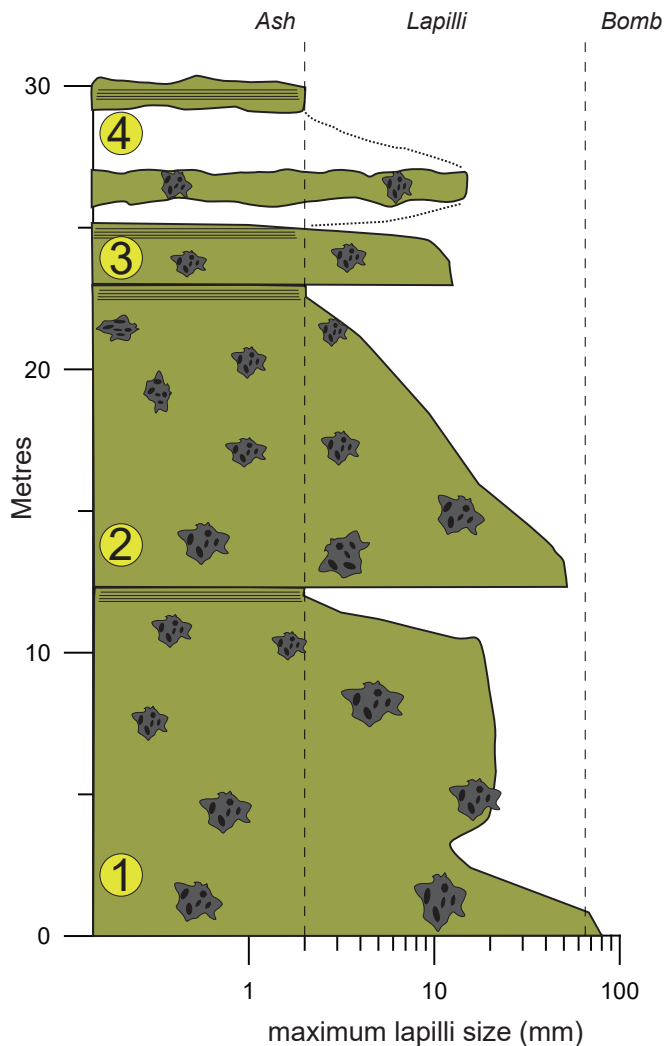


Fig. 5. Measured section of cliff shown in Fig. 3. The numbers on yellow background refer to the four fining-upward sequences.

exposed on its southern and northern flanks. The Middle Scud body on the west side of the Hickman pluton, ~15 km west of Mount Hickman ultramafic complex, contains sheared and pervasively serpentinized biotite-rich peridotite.

3. Methods

3.1. $^{40}\text{Ar}/^{39}\text{Ar}$ methodology

Laser $^{40}\text{Ar}/^{39}\text{Ar}$ step-heating analysis was carried out at the Geological Survey of Canada Noble Gas laboratory in Ottawa, Ontario. Unaltered pieces (0.25-1.0 mm) of hornblende were picked from four gabbroic to granodioritic samples of the Hickman pluton (Stikine suite). Individual hornblende separates were loaded into aluminum foil packets along with grains of Fish Canyon Tuff Sanidine (FCT-SAN) to act as flux monitor (apparent age = 28.201 ± 0.023 Ma; 1σ , Kuiper et al., 2008). The sample packets were arranged radially inside an aluminum canister. The samples were submitted for a 60 MWh irradiation in high flux position 5c at the research reactor of McMaster University in Hamilton, Ontario, Canada.

Upon return from the reactor, samples were split into one or more aliquots each and loaded into individual 1.5 mm-diameter holes in a copper planchet. The planchet was then placed in the extraction line and the system evacuated. Heating of individual sample aliquots in steps of increasing temperature was achieved using a MerchanteK MIR10 10W CO_2 laser equipped with a 2 mm x 2 mm flat-field lens. The released Ar gas was cleaned in the extractions line over two hot SAESTTM NP-10 getters of St 707 alloy (Zr-V-Fe) held at ~400°C (to remove nitrogen, oxygen, hydrocarbons, water and other active gases) and a room-temperature getter containing HY-STOR[®] 201 calcium-nickel alloy pellets (to remove hydrogen), and then analyzed isotopically using a Nu Instruments Noblesse noble gas mass spectrometer, equipped with a Faraday detector and three ion counters. For the first aliquots of each sample, the analyses were run in single ion counter peak-hopping mode for small signals ('SC' mode as described in Kellett and Joyce, 2014), and in cases where the ^{40}Ar signal exceeded ion counting tolerance, a Faraday plus single ion counter peak-hopping routine was used. For Aliquot #2 of sample ZE09-059A all steps were run in ion counter multi-collection mode ('MC-Y' mode of Kellett and Joyce, 2014), except for the 7.5W step for which the ^{40}Ar signal exceeded the ion counter tolerance. This step was run using full multi-collection mode ('MC-O' mode of Kellett and Joyce, 2014). Baselines were measured before each analysis. Blank measurements were made throughout the analytical sessions (Table 1). Mass fractionation and detector efficiencies were determined from repeated measurements of air aliquots, whereby ^{40}Ar and ^{36}Ar signals were measured on all collectors. $^{40}\text{Ar}/^{36}\text{Ar}$ ratios were then determined for each collector individually, and for each combination of collectors (excluding ^{40}Ar on the Faraday/ ^{36}Ar on each ion counter). Raw data from the mass spectrometer were processed using in-house Excel[®] data handling macros that use average, linear or non-linear regression protocols based on the equations of Koppers (2002).

Error analysis on individual steps follows numerical error analysis routines outlined in Scailliet (2000); error analysis on grouped data follows algebraic methods of Roddick (1988). Corrected argon isotopic data are listed in Table 1, and presented in Figure 7 as spectra of gas release or inverse-isochron plots per Roddick et al. 1980. In the case of sample ZE09-059A for which two aliquots were run, the spectrum plotted contains step-heating data from both aliquots, alternately shaded and normalized to the total volume of ^{39}Ar released for each aliquot. Such plots provide a visual image of replicated heating profiles, evidence for ^{40}Ar -loss in the low temperature steps, and the error and apparent age of each step. Reported plateau ages are defined as ages derived from three or more consecutive heating steps that are statistically equivalent, and comprise greater than 50% of the total ^{39}Ar released. MSWD is defined as the mean square of weighted deviates.

Neutron flux gradients throughout the sample canister were evaluated by analyzing the FCT-SAN sanidine flux monitors included with each sample packet and interpolating a linear

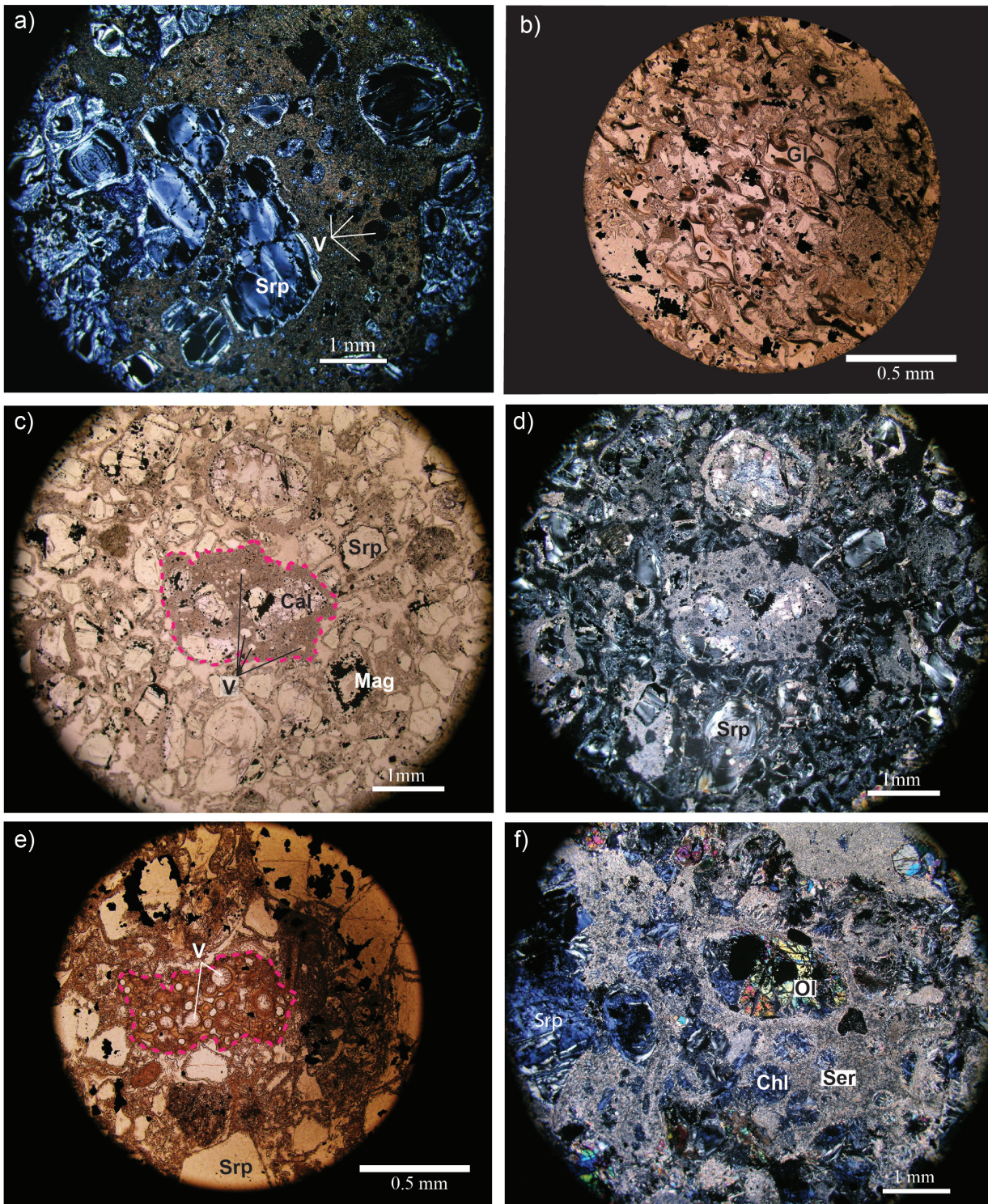


Fig. 6. **a)** Cross-polarized photomicrograph of a lapilli composed of mm-scale pervasively serpentinized olivine (Srp) that contains fine euhedra of magnetite set in a scoriaceous, very fine-grained groundmass of devitrified glass. Sample 1. **b)** Plane-polarized light image of an ash tuff at the top of fining-upward sequence 1 (Figs. 3 and 5). Concavo-convex, bubble-wall shards of clear to light brown, partially palagonitized, glass (Gl) comprise >40% of the rock. **c)** and **d)** Plane and cross-polarized images of a vesicular lapilli tuff (Sample 4). Olivine, both as part of larger lapilli or as individual crystals has been completely replaced by serpentine, magnetite, and calcite. Dashed pink line in **c)** outlines the margin of a ~2 mm lapilli. **e)** Plane-polarized light image of a palagonitized lapillus of scoria (dark brown outlined by dashed pink line) in crystal-rich ash tuff at the top of fining-upward sequence 4. **f)** Cross-polarized photomicrograph of a lapilli tuff from the Yehiniko occurrence, previously interpreted as a Polaris suite intrusion. Although the sample has been extensively altered to serpentine (after olivine), sericite, and chlorite, relict fresh olivine is abundant. Cal: calcite, Chl: chlorite, Mag: magnetite, Ol: olivine, Ser: sericite, Srp: serpentine, V: vesicle (now infilled by chlorite).

Table 1. CO₂ laser step-heating ⁴⁰Ar/³⁹Ar data. All uncertainties quoted at 2σ level unless otherwise indicated.

Power ^a	Volume ³⁹ Ar x10 ¹¹ cc	³⁶ Ar/ ³⁹ Ar	±	³⁷ Ar/ ³⁹ Ar	±	³⁸ Ar/ ³⁹ Ar	±	⁴⁰ Ar/ ³⁹ Ar	±	⁴⁰ Ar/ ³⁹ Ar	±	f _g ^c (%)	App. Age Ma ^d	±	³⁹ Ar/ ⁴⁰ Ar	± % 1σ	³⁶ Ar/ ⁴⁰ Ar	± % 1σ	r		
ZE09-059A Hornblende; J=00745300^b Hickman pluton (Z10118) Inverse Isochron Age = 211.3 ± 4.4 Ma (Aliquots 1 and 2 combined; Lat/Long 57.31425/-131.11436)																					
Aliquot: 1																					
3.0	0.0016	0.2208	0.0082	6.533	0.167	0.697	0.019	86.596	1.580	75.3	21.359	2.666	0.7	268.3	30.9	#	0.011548	0.912416	0.002549	1.930474	0.311898
3.5	0.0020	0.0996	0.0062	6.649	0.161	0.169	0.012	40.497	1.112	72.7	11.070	2.077	0.8	143.9	25.8	#	0.024693	1.372093	0.002459	3.309592	0.361799
3.9	0.0122	0.0622	0.0015	3.751	0.062	0.219	0.012	29.878	0.290	61.5	11.512	0.511	4.9	149.5	6.3	#	0.033469	0.485716	0.002080	1.264929	0.319293
4.2	0.0188	0.0188	0.0018	8.555	0.130	0.406	0.013	22.791	0.191	24.4	17.237	0.548	5.2	219.5	6.5	#	0.043876	0.419025	0.000825	4.672295	0.067683
4.6	0.0156	0.0090	0.0018	9.281	0.139	0.483	0.014	19.138	0.155	13.9	16.480	0.538	6.3	210.4	6.5	#	0.052252	0.404058	0.000470	9.731073	0.032548
5.0	0.0086	0.0132	0.0021	9.446	0.152	0.335	0.012	20.112	0.293	19.4	16.204	0.687	3.5	207.0	8.2	#	0.049721	0.727794	0.000658	8.019058	0.079435
5.5	0.0063	0.0046	0.0019	11.530	0.164	0.470	0.013	18.715	0.068	7.2	17.364	0.578	26.8	221.0	6.9	#	0.053433	0.182771	0.000244	21.246425	0.005697
6.0	0.0184	0.0037	0.0019	10.650	0.158	0.482	0.013	17.371	0.142	6.3	16.274	0.579	7.4	207.9	7.0	#	0.057566	0.408461	0.000214	25.620646	0.013512
6.5	0.0058	0.0087	0.0027	11.017	0.186	0.332	0.013	18.306	0.422	14.1	15.733	0.912	2.3	201.3	11.0	#	0.054626	1.152899	0.000476	15.778934	0.067746
7.5	0.0366	0.0075	0.0018	10.614	0.155	0.561	0.013	19.256	0.107	11.5	17.047	0.548	14.8	217.2	6.5	#	0.051931	0.278605	0.000388	12.172776	0.014745
15.0	0.0679	0.0024	0.0013	7.390	0.106	0.384	0.012	15.782	0.062	4.4	15.082	0.375	27.4	193.4	4.5	#	0.063364	0.197334	0.000150	26.440008	0.004635
Aliquot: 2																					
3.0	0.0015	0.1614	0.0078	8.903	3.040	-0.041	-0.013	65.022	1.427	73.3	17.335	2.673	1.3	220.6	31.8	#	0.015379	1.097767	0.002482	2.620440	0.397138
3.5	0.0013	0.0435	0.0078	6.917	3.120	-0.019	-0.011	28.091	1.643	45.8	15.228	2.816	1.1	195.2	34.0	#	0.035598	2.920999	0.001550	9.405879	0.298149
3.9	0.0013	0.0586	0.0076	6.572	4.081	-0.022	-0.011	32.609	1.569	53.1	15.289	2.717	1.1	195.9	32.8	#	0.030666	2.405271	0.001797	6.875240	0.335012
4.2	0.0012	0.0631	0.0081	3.483	3.611	-0.023	-0.012	34.478	1.675	54.1	15.836	2.888	1.0	202.6	34.7	#	0.029004	2.427671	0.001830	6.809965	0.334779
4.6	0.0009	0.0504	0.0118	10.140	4.494	-0.021	-0.011	32.598	2.405	45.7	17.693	4.203	0.8	224.9	49.9	#	0.030677	3.682431	0.001547	12.194885	0.290518
5.0	0.0042	0.0219	0.0027	9.315	0.977	-0.015	-0.011	23.050	0.521	28.0	16.589	0.938	3.5	211.7	11.2	#	0.043384	1.129425	0.000949	6.179897	0.169426
5.5	0.0087	0.0063	0.0020	10.521	0.800	-0.012	-0.011	18.892	0.256	9.8	17.037	0.654	7.3	217.1	7.8	#	0.052933	0.677719	0.000332	16.247860	0.040730
6.0	0.0112	0.0278	0.0024	13.168	0.685	-0.016	-0.011	26.219	0.214	31.4	17.993	0.748	9.4	228.5	8.9	#	0.038140	0.408809	0.001062	4.389982	0.076225
6.5	0.0205	0.0028	0.0020	11.843	0.512	-0.012	-0.011	17.356	0.117	4.8	16.527	0.615	17.3	210.9	7.4	#	0.057618	0.337498	0.000162	36.416034	0.010434
7.5	0.0573	0.0050	0.0017	10.155	0.369	0.781	0.011	18.492	0.074	8.1	17.003	0.513	48.3	216.7	6.1	#	0.054078	0.201232	0.000272	17.050653	0.012445
15.0	0.0106	0.0178	0.0017	9.435	0.502	-0.014	-0.011	21.101	0.215	24.9	15.837	0.548	8.9	202.6	6.6	#	0.047392	0.509907	0.000844	4.833784	0.092081
ZE09-059B Hornblende; J=.00733680^b Hickman pluton (Z10119) Plateau Age = 222.2 ± 2.8 Ma; Lat/Long 57.31425/-131.11436																					
Aliquot: 1																					
3.0	0.0033	0.2114	0.0050	4.462	0.108	0.509	0.015	75.991	0.903	82.2	13.531	1.589	1.0	171.9	19.1	#	0.013160	0.594127	0.002782	1.226595	0.306170
3.5	0.0011	0.0415	0.0105	1.008	0.148	0.063	0.014	26.115	2.178	46.9	13.865	3.780	0.3	175.9	45.4	#	0.038292	4.160458	0.001587	13.342852	0.300559
3.9	0.0039	0.0926	0.0036	3.036	0.080	0.183	0.012	41.493	0.662	66.0	14.115	1.213	1.2	178.9	14.6	#	0.024101	0.797124	0.002233	2.050648	0.317603
4.2	0.0032	0.0282	0.0037	1.691	0.072	0.058	0.011	24.028	0.767	34.7	15.685	1.323	1.0	197.8	15.7	#	0.041618	1.595115	0.001175	6.713847	0.218813
4.6	0.0042	0.0236	0.0028	2.756	0.075	0.091	0.011	23.391	0.584	29.9	16.403	1.004	1.3	206.3	11.9	#	0.042752	1.247268	0.001011	6.028879	0.188436
5.0	0.0233	0.0170	0.0018	10.384	0.152	0.531	0.014	22.543	0.124	22.3	17.521	0.557	7.0	219.6	6.5	#	0.044360	0.275155	0.000754	5.424043	0.037195
5.5	0.0628	0.0055	0.0016	9.525	0.137	0.689	0.015	19.595	0.077	8.3	17.966	0.482	18.9	224.8	5.6	#	0.051034	0.197007	0.000281	14.633255	0.066711
6.0	0.1195	0.0014	0.0014	8.455	0.119	0.784	0.016	18.086	0.048	2.4	17.659	0.422	36.0	221.2	5.0	#	0.055290	0.132764	0.000080	49.138802	0.001945
6.5	0.0454	0.0025	0.0016	9.281	0.134	0.702	0.015	18.578	0.096	4.0	17.840	0.476	13.7	223.4	5.6	#	0.053827	0.257479	0.000134	31.637550	0.005272
7.5	0.0376	0.0020	0.0016	9.526	0.138	0.688	0.015	18.292	0.098	3.3	17.697	0.491	11.3	221.7	5.8	#	0.054668	0.267584	0.000110	40.387244	0.005074
15.0	0.0273	0.0052	0.0019	10.721	0.156	0.723	0.016	18.032	0.107	8.5	16.508	0.558	8.2	207.6	6.6	#	0.055456	0.295821	0.000286	17.988349	0.012374

Table 1. Continued.

Power ^a ³⁹ Ar/ ³⁹ Ar	Volume ³⁹ Ar/ ³⁹ Ar	±	³⁹ Ar/ ³⁹ Ar	±	³⁸ Ar/ ³⁹ Ar	±	⁴⁰ Ar/ ³⁹ Ar	±	% ⁴⁰ Ar ATM	f ^c Age (%)	App. Age	±	³⁹ Ar/ ⁴⁰ Ar	± % 1σ	Inverse Isochron Data ³⁹ Ar/ ⁴⁰ Ar	± % 1σ	r				
ZrE09-060 Hornblende; J=00733080^b Hickman pluton (Z10120) Inverse Isochron Age = 221.6 ± 2.5 Ma; Lat/Long 57.31402/-131.0485																					
Aliquot: 1																					
3.0	0.0006	0.2019	0.0183	2.853	0.351	0.586	0.026	93.165	3.430	64.0	33.495	5.941	0.2	398.9	63.1	0.010734	1.840114	0.002167	4.624446	0.243954	
3.5	0.0004	0.1764	0.0250	3.403	0.511	0.187	0.022	72.391	4.390	72.0	20.253	8.261	0.2	251.4	95.1	#	0.013814	3.029287	0.002437	7.464110	0.322080
3.9	0.0006	0.0759	0.0154	2.695	0.340	0.050	0.016	41.683	2.692	53.8	19.264	5.204	0.2	239.9	60.3	#	0.023991	3.225428	0.001820	10.544903	0.270588
4.2	0.0002	0.0982	0.0395	0.629	0.785	0.019	0.029	42.518	6.655	68.3	13.496	13.367	0.1	171.3	160.9	#	0.023519	7.760209	0.002310	21.500451	0.351557
4.6	0.0004	0.0638	0.0261	2.896	0.538	0.135	0.021	35.757	4.400	52.7	16.897	8.799	0.2	212.0	103.6	#	0.027966	6.121814	0.001785	21.218806	0.272693
5.0	0.0007	0.0925	0.0156	6.033	0.332	0.417	0.020	46.508	2.979	58.8	19.183	5.389	0.3	238.9	62.5	#	0.021502	3.198464	0.001988	8.896333	0.326352
5.5	0.0050	0.0138	0.0026	7.464	0.141	0.543	0.015	23.791	4.440	17.1	19.720	0.894	2.0	245.2	10.3	#	0.042033	0.924750	0.000579	9.644968	0.085019
6.0	0.0906	0.0010	0.0010	5.908	0.086	0.497	0.013	18.086	0.048	1.6	17.794	0.299	36.3	222.6	3.5	#	0.055292	0.132186	0.000055	50.528258	0.001795
6.5	0.0408	0.0050	0.0011	6.527	0.098	0.499	0.013	19.556	0.098	7.6	18.067	0.352	16.4	225.9	4.1	#	0.051136	0.250952	0.000258	11.373677	0.012452
7.5	0.0886	0.0013	0.0009	5.549	0.081	0.514	0.013	18.216	0.056	2.1	17.839	0.283	35.5	223.2	3.3	#	0.054896	0.153044	0.000070	36.861940	0.001937
15.0	0.0215	0.0007	0.0012	6.384	0.098	0.542	0.014	17.435	0.112	1.2	17.219	0.370	8.6	215.9	4.4	#	0.057355	0.320644	0.000042	81.517722	0.003218
ZrE09-061 Hornblende; J=00732860^b Hickman pluton (Z10121) Plateau Age = 220.1 ± 2.7 Ma; Lat/Long 57.29168/-131.0655																					
Aliquot: 1																					
3.0	0.0015	0.3463	0.0100	6.950	0.217	0.575	0.018	125.286	2.076	81.7	22.944	3.051	0.5	282.2	34.5	#	0.007982	0.828357	0.002764	1.430357	0.265033
3.5	0.0008	0.1506	0.0117	4.784	0.285	0.069	0.015	57.791	2.676	77.0	13.290	4.193	0.3	168.7	50.5	#	0.017304	2.313974	0.002606	4.351875	0.462234
3.9	0.0014	0.1253	0.0093	3.022	0.181	0.056	0.013	51.597	1.673	71.8	14.560	3.108	0.5	184.1	37.1	#	0.019381	1.620493	0.002429	3.935871	0.340305
4.2	0.0016	0.1062	0.0076	3.114	0.155	0.060	0.012	45.125	1.408	69.5	13.752	2.569	0.6	174.3	30.9	#	0.022161	1.559292	0.002353	3.807931	0.344145
4.6	0.0014	0.0316	0.0081	3.348	0.163	0.087	0.013	25.041	1.513	37.3	15.691	2.821	0.5	197.6	33.5	#	0.039935	3.016409	0.001264	13.154075	0.217199
5.0	0.0033	0.0391	0.0038	7.191	0.157	0.308	0.013	28.199	0.685	41.0	16.632	1.294	1.1	208.8	15.3	#	0.035462	1.214483	0.001388	4.945848	0.219408
5.5	0.0169	0.0142	0.0017	9.267	0.142	0.448	0.013	21.698	0.149	19.3	17.505	0.509	5.8	219.2	6.0	#	0.046088	0.343806	0.000654	5.827378	0.044984
6.0	0.0799	0.0022	0.0017	10.164	0.152	0.402	0.012	18.368	0.106	3.5	17.719	0.516	27.5	221.7	6.0	#	0.054443	0.288156	0.000119	38.978379	0.004034
6.5	0.1050	0.0021	0.0013	8.005	0.116	0.417	0.012	18.326	0.051	3.4	17.703	0.401	36.1	221.5	4.7	#	0.054568	0.138103	0.000115	31.939381	0.002550
7.5	0.0409	0.0010	0.0011	6.141	0.092	0.386	0.012	17.850	0.094	1.6	17.562	0.330	14.1	219.8	3.9	#	0.056023	0.263024	0.000055	54.996033	0.003435
15.0	0.0382	0.0013	0.0013	7.660	0.113	0.476	0.013	17.067	0.074	2.3	16.679	0.397	13.1	209.4	4.7	#	0.058591	0.215781	0.000077	50.325217	0.003141

^a As measured by laser in % of full nominal power (10W). Ages marked with an asterisk (*) or a pound symbol (#) were those used in the plateau or inverse isochron age calculation, respectively.

^b Nominal J (±0.30%, 1σ) from GSC Irradiation Batch #61, referenced to Fish Canyon Tuff Sandine=28.201 ±0.023 Ma (1σ, Kuiper et al., 2008).

^c Fraction ³⁹Ar as percent of gas in all aliquots.

^d Errors on ages from each heating step are analytical only and do not reflect error in irradiation parameter J.

Plateau and inverse isochron age errors are quoted at 2σ and incorporate the error in J, but not the error in decay constants

Atmospheric ⁴⁰Ar/³⁶Ar=295.5

Decay Constant (⁴⁰K λ_{total})=5.463 ±0.214 × 10⁻¹⁰/yr (2σ, Min et al., 2000)

Blanks were measured before and after aliquot analysis and levels varied between ⁴⁰Ar=2.5*10⁻⁷ to 3.9*10⁻⁷ nmol, ³⁹Ar=1.8*10⁻¹⁰ to 5.4*10⁻¹⁰ nmol, ³⁸Ar=1.8*10⁻¹⁰ to 1.4*10⁻⁹ nmol, ³⁷Ar=1.3*10⁻⁹ to 2.3*10⁻⁹ nmol, ³⁶Ar=1.1*10⁻⁹ to 1.4*10⁻⁹ nmol, all at ±10 % uncertainty (2σ). Nucleogenic interference corrections (±2σ) are (⁴⁰Ar/³⁹Ar)K=0.025 ±0.005, (³⁸Ar/³⁹Ar)K=0.011 ±0.010, (⁴⁰Ar/³⁷Ar)Ca=0.002 ±0.002, (³⁹Ar/³⁷Ar)Ca=0.00068 ±0.00004, (³⁸Ar/³⁷Ar)Ca=0.00003 ±0.00003, (³⁶Ar/³⁷Ar)Ca=0.00028 ±0.00016.

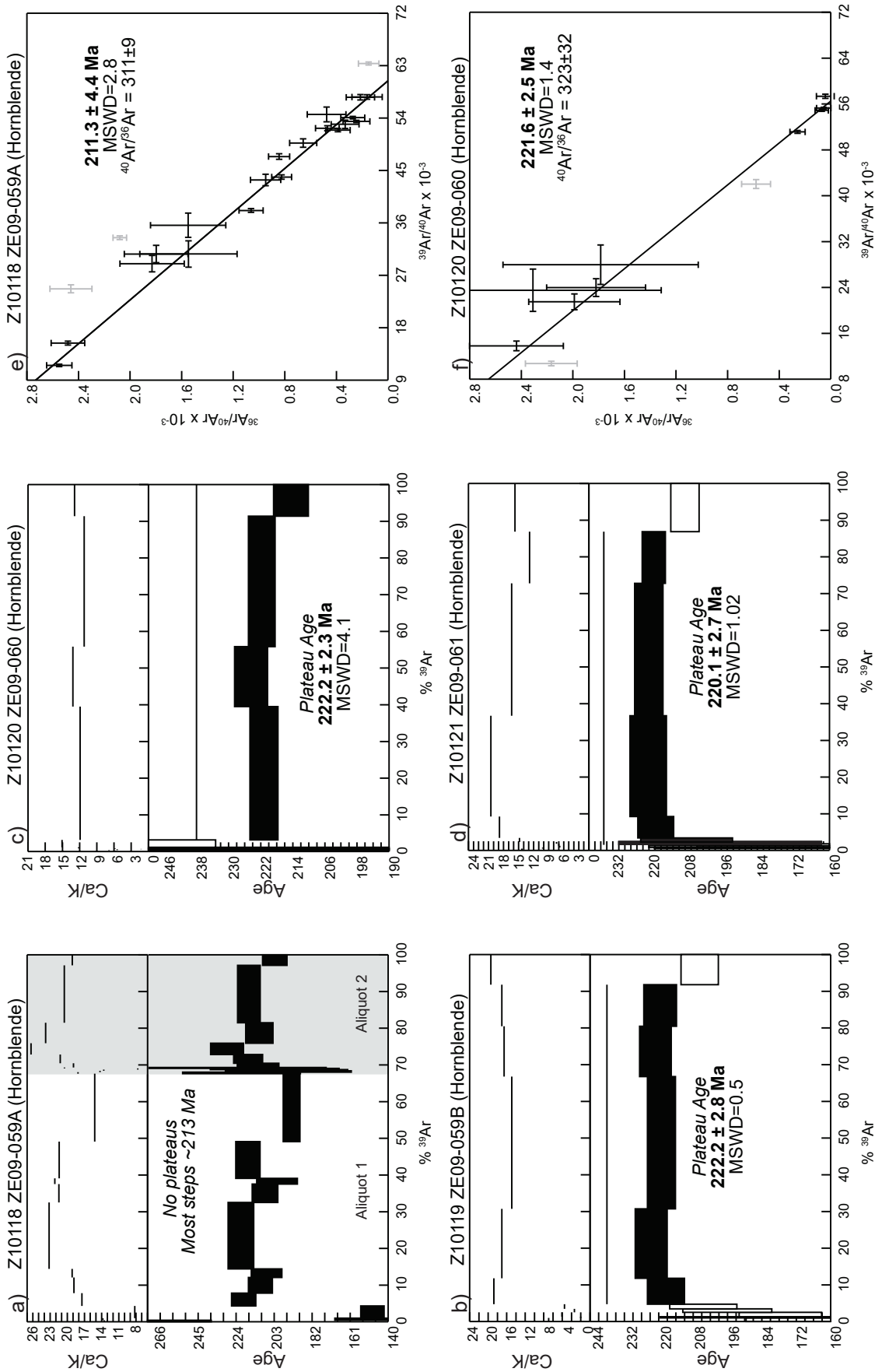


Fig. 7. Hornblende $^{40}\text{Ar}/^{39}\text{Ar}$ age spectra and Ca/K ratios as a function of stepped release of ^{39}Ar during heating of samples: **a)** ZE09-059A, **b)** ZE09-059B, **c)** ZE09-060, and **d)** ZE09-061. Inverse $^{36}\text{Ar}/^{40}\text{Ar}$ vs. $^{39}\text{Ar}/^{40}\text{Ar}$ isochron diagrams for samples: **e)** ZE09-059A and **f)** ZE09-060, respectively.

fit against calculated J-factor and sample position. The error on individual J-factor values is conservatively estimated at $\pm 0.6\%$ (2σ). Because the error associated with the J-factor is systematic and unrelated to individual analyses, correction for this uncertainty is not applied until ages from isotopic correlation diagrams are calculated (Roddick, 1988). Errors in the plateau and inverse isochron ages do not include the errors of decay constants. Nucleogenic interference corrections were $(^{40}\text{Ar}/^{39}\text{Ar})_{\text{K}} = 0.025 \pm 0.005$, $(^{38}\text{Ar}/^{39}\text{Ar})_{\text{K}} = 0.011 \pm 0.010$, $(^{40}\text{Ar}/^{37}\text{Ar})_{\text{Ca}} = 0.002 \pm 0.002$, $(^{39}\text{Ar}/^{37}\text{Ar})_{\text{Ca}} = 0.00068 \pm 0.00004$, $(^{38}\text{Ar}/^{37}\text{Ar})_{\text{Ca}} = 0.00003 \pm 0.00003$, $(^{36}\text{Ar}/^{37}\text{Ar})_{\text{Ca}} = 0.00028 \pm 0.00016$. The decay constant used was $^{40}\text{K} \lambda_{\text{total}} = 5.463 \pm 0.214 \times 10^{-10}/\text{a}$ (2σ) from Min et al. (2000). All errors are quoted at the 2σ level of uncertainty.

3.2. Major and trace element geochemistry

We analyzed 11 samples of Middle-Late Triassic ultramafic rocks that were collected during reconnaissance work in 2009-2011 (Fig. 2). Eight samples from four localities are olivine tuff. One sample, from the Mount Hickman ultramafic complex, is a phlogopite clinopyroxenite. Two clasts of augite-phyric picrite were collected from a diatreme that cuts the Hickman pluton.

The samples were crushed and processed using lithium metaborate/tetraborate fusion and nitric acid dissolution and analyzed using inductively coupled plasma-optical emission spectrometry (ICP-OES) and inductively coupled plasma-mass spectrometry (ICP-MS) at Activation Laboratories (Ancaster, Ontario; 4Lithores analytical package). At a 95% confidence level, the uncertainty in measurement of major elements, significantly exceeding their quantitation limit (defined as 3.33 times the detection limit), is $\leq 4\%$ relative. The uncertainty in Na_2O , K_2O , and P_2O_5 , which are present in low abundances, is significantly larger ranging between 5 and 30% relative at a 95% confidence level. With the exception of Rb, Pb, Nb, Ta, and Tm, trace elements concentrations in most samples exceed their quantitation limits. The uncertainty in individual measurements, at a 95% confidence level, for transitional metals (e.g. Ni, Cr) is $< 20\%$. The relative uncertainty in measurement of rare earth elements (REE) and high field strength elements, at a 95% confidence interval is typically $< 35\%$.

4. Results

4.1. $^{40}\text{Ar}/^{39}\text{Ar}$ results

Sample ZE09-059A is a medium-grained plagioclase porphyritic hornblende-biotite granodiorite. Hornblende occurs as variably altered grains and as fresh hornblende-magnetite clusters. Two aliquots of fresh hornblende were analyzed; both giving disturbed spectra from which no age could be interpreted. Most of the steps, however, fall in the ~ 213 Ma age range (Fig. 7a; Table 1). Data points on the inverse isochron diagram are generally collinear, plotting along a line that intersects the y-axis at a nearly-atmospheric $^{40}\text{Ar}/^{36}\text{Ar}$ composition of 311 ± 9 and yields an age of 211.2 ± 4.4 Ma (Fig. 7e; MSWD = 2.8). We interpret that this is the best approximation of the hornblende cooling age for this sample. Imprecision of the age is due, in

part, to elevated and variable Ca/K in the sample; the Ca/K values range between ~ 7 and 25 (Fig. 7a), suggesting that the grains are compositionally inhomogeneous.

Sample ZE09-059B is from rounded to amoeboid diorite enclaves in medium-grained plagioclase porphyritic hornblende-biotite granodiorite. Hornblende from this sample was clean, fresh, and dark brown to black. One aliquot was analyzed and, although it yielded a slightly hump-shaped spectrum, a robust plateau was obtained for five mid- to high-temperatures steps (excluding the fusion step), giving an age of 222.2 ± 2.8 Ma (Fig. 7b; MSWD = 0.5, 87% of total ^{39}Ar). This is the preferred cooling age of the Hickman pluton at this locality.

Sample ZE09-060 is a weakly-foliated, medium-grained, hornblende-biotite diorite. Weakly-zoned hornblende locally contains altered biotite inclusions. Hornblende from this sample selected for analysis was clean, fresh, and dark brown to black. One aliquot was analyzed, and yielded a plateau with four highest-temperatures steps, giving an age of 222.2 ± 2.3 Ma (Fig. 7c; MSWD = 4.1, 97% of total ^{39}Ar). When plotted on the inverse isochron diagram, nearly all of the data (9 of 11 heating steps) plot along a line that regresses to an essentially atmospheric $^{40}\text{Ar}/^{36}\text{Ar}$ composition of 323 ± 32 , and gives an age of 221.6 ± 2.5 Ma (Fig. 7f; MSWD = 1.4). Although indistinguishable from the plateau age, the isochron age includes almost all of the heating steps and has a more acceptable MSWD, and is therefore the preferred cooling age for this sample. This age is indistinguishable from that of sample ZE09-059B (Fig. 7b).

Sample ZE09-061 is a medium-grained to pegmatitic hornblende gabbro. Weakly zoned hornblende is variably altered and locally contains altered biotite inclusions. One aliquot was analyzed, yielding a slightly hump-shaped release spectrum. Six mid- to high-temperatures steps, however, give a plateau age of 220.1 ± 2.7 Ma (Fig. 7d; MSWD = 1.02, 85% of total ^{39}Ar). The fusion step, which gives an apparent age of 209 ± 5 Ma, was not included.

4.2. Geochemistry

Pyroclastic samples have high volatile contents (7-13 wt.% LOI; Table 2) that reflect, in part, extensive serpentinization of olivine. All pyroclastic samples have high concentrations of MgO (29-38 wt.%, LOI-free) and Ni (1100-1700 ppm), low concentrations of Al_2O_3 (4-6 wt.%) and, with the exception of sample 9, low concentrations of alkalis ($\text{Na}_2\text{O} + \text{K}_2\text{O} \leq 0.3$ wt.%). The high absolute MgO and Ni-Cr concentrations and strong negative correlations between MgO and the relatively immobile, conserved oxides (Al_2O_3 , TiO_2 , P_2O_5 ; not shown) suggest that the geochemical variability among the ultramafic pyroclastic rocks is mainly controlled by accumulation of olivine. Samples define a nearly vertical array that projects towards $\sim \text{Fo}_{90}$ on Mg vs. Fe cation unit plot, along an olivine control line (Fig. 8a). Primary liquid compositions were calculated by fractional removal of olivine from each sample at upper crustal pressure ($P = 0.1$ GPa) until the resulting parental

Table 2. Major and trace element compositions of Late Triassic ultramafic rocks; detection limits in parentheses.

Sample #	1	2	3	4	5	6	7	8	9	10	11
	ZE11-649A	ZE11-649D	ZE11-649F	ZE11-648C	ZE11-648D	ZE11-644A	ZE11-644B	ZE11-645A	ZE11-645B	ZE10-172	ZE09-062
Eastings	381572	381572	381572	386785	386785	363411	363411	360072	360072	359306	374025
Northings	6347256	6347256	6347256	6350227	6350227	6338573	6338573	6341804	6341804	6347258	6347258
Unit	Stuhini	Stuhini	Stuhini	Stuhini	Stuhini	clast	clast	Stuhini	Stuhini	Stuhini	Polaris suite
Lithology	lapilli tuff	Augite picrite	Augite picrite	lapilli tuff	lapilli tuff	lapilli tuff	olivine clinopyroxenite				
Major elements (wt. %)											
SiO ₂ (0.01)	40.72	40.1	39.98	39.18	39.57	45.6	42.43	40.25	42.46	41.81	44.25
TiO ₂ (0.001)	0.21	0.27	0.26	0.20	0.31	0.62	0.43	0.20	0.26	0.28	0.91
Al ₂ O ₃ (0.01)	3.97	4.57	4.30	3.82	4.82	9.79	7.99	3.57	5.12	4.70	4.41
Fe ₂ O ₃ (0.01)	9.28	9.53	9.48	8.71	9.39	9.02	9.17	9.25	9.72	9.55	18.62
MnO (0.001)	0.14	0.15	0.14	0.09	0.12	0.15	0.16	0.13	0.15	0.16	0.20
MgO (0.01)	31.69	29.22	29.9	30.9	25.52	15.42	21.35	33.84	29.47	29.06	13.69
CaO (0.01)	4.64	6.37	5.83	3.26	9.00	8.61	8.85	3.06	4.44	4.63	16.81
Na ₂ O (0.01)	0.03	0.08	0.08	0.07	0.05	1.35	0.22	0.17	0.73	0.22	0.48
K ₂ O (0.01)	0.24	0.17	0.14	0.05	0.04	2.81	0.44	0.02	0.65	0.03	0.45
P ₂ O ₅ (0.01)	0.08	0.09	0.09	0.06	0.13	0.42	0.37	0.05	0.08	0.1	0.02
LOI	9.78	10.11	10.25	13.48	10.71	3.86	8.16	8.54	7.39	7.71	0.53
Total (0.01)	100.80	100.60	100.50	99.82	99.66	97.65	99.57	99.09	100.50	98.25	100.40
Trace elements (ppm)											
Cs (0.1)	0.2	0.8	0.5	2.1	1.0	4.5	3.3	0.1	1.1	1.2	0.6
Rb (1)	5	6	3	4	2	84	23	<1	11	2	10
Ba (3)	138	146	252	59	68	744	118	48	95	13	140
Th (0.05)	0.17	0.25	0.19	0.22	0.32	1.58	1.24	0.47	0.34	0.15	0.09
U (0.01)	0.10	0.17	0.13	0.11	0.19	0.97	0.78	0.16	0.23	0.16	0.29
Nb (0.2)	0.3	0.7	0.2	0.5	0.7	3.1	1.8	0.8	0.7	<0.2	1.0
Ta (0.01)	<0.01	0.13	0.41	<0.01	0.02	0.14	0.07	<0.01	0.01	<0.01	0.04
Pb (5)	<5	<5	<5	<5	<5	<5	<5	<5	<5	<5	<5
Sr (2)	103	183	113	198	94	412	85	73	208	66	113
Zr (1)	10	12	12	10	17	48	34	27	12	14	20
Hf (0.1)	0.30	0.40	0.30	0.30	0.50	1.30	1.00	0.70	0.30	0.40	0.70
Y (0.5)	4.4	5.3	5.0	4.0	7.1	13.7	9.7	4.3	5.4	4.9	8.9
Ga (1)	5	4	4	4	4	11	8	5	6	5	11
Sc (1)	16	18	18	14	21	27	21	15	18	19	76
V (5)	101	123	104	72	106	210	185	98	97	123	461
Co (1)	60	60	60	70	60	70	70	60	60	70	90
Zn (30)	98	93	92	97	81	54	69	102	94	94	72
Cu (10)	40	50	40	30	70	70	70	20	50	30	50
Cr (20)	2120	2190	1950	1750	1660	950	1660	2400	2100	2120	280
Ni (20)	1540	1380	1340	1560	1120	580	1070	1700	1380	1260	170
La (0.05)	1.62	2.74	1.86	2.23	3.15	8.35	6.35	5.31	3.41	1.36	1.80
Ce (0.05)	3.55	5.96	4.26	4.76	6.68	18.00	13.80	11.00	7.18	3.56	4.66
Pr (0.01)	0.46	0.72	0.55	0.57	0.82	2.21	1.66	1.19	0.84	0.52	0.77
Nd (0.05)	2.23	3.16	2.69	2.62	4.17	10.20	7.51	4.34	3.51	2.33	4.19
Sm (0.01)	0.60	0.84	0.64	0.63	1.13	2.42	1.83	0.90	0.82	0.58	1.50
Eu (0.005)	0.216	0.286	0.260	0.219	0.365	0.815	0.569	0.248	0.315	0.128	0.473
Gd (0.01)	0.74	0.92	0.86	0.77	1.29	2.66	1.83	0.86	0.77	0.77	1.74
Tb (0.01)	0.13	0.17	0.14	0.13	0.20	0.45	0.33	0.15	0.18	0.11	0.31
Dy (0.01)	0.73	0.95	0.88	0.67	1.16	2.50	1.83	0.74	0.94	0.74	1.74
Ho (0.01)	0.16	0.20	0.17	0.13	0.25	0.49	0.35	0.17	0.18	0.14	0.31
Er (0.01)	0.44	0.61	0.52	0.42	0.66	1.44	1.04	0.48	0.57	0.42	0.88
Tm (0.05)	0.060	0.071	0.073	0.064	0.104	0.212	0.138	0.063	0.088	0.065	0.133
Yb (0.01)	0.42	0.60	0.51	0.43	0.60	1.43	1.02	0.45	0.61	0.47	0.82
Lu (0.002)	0.060	0.085	0.079	0.057	0.103	0.228	0.154	0.073	0.073	0.075	0.113

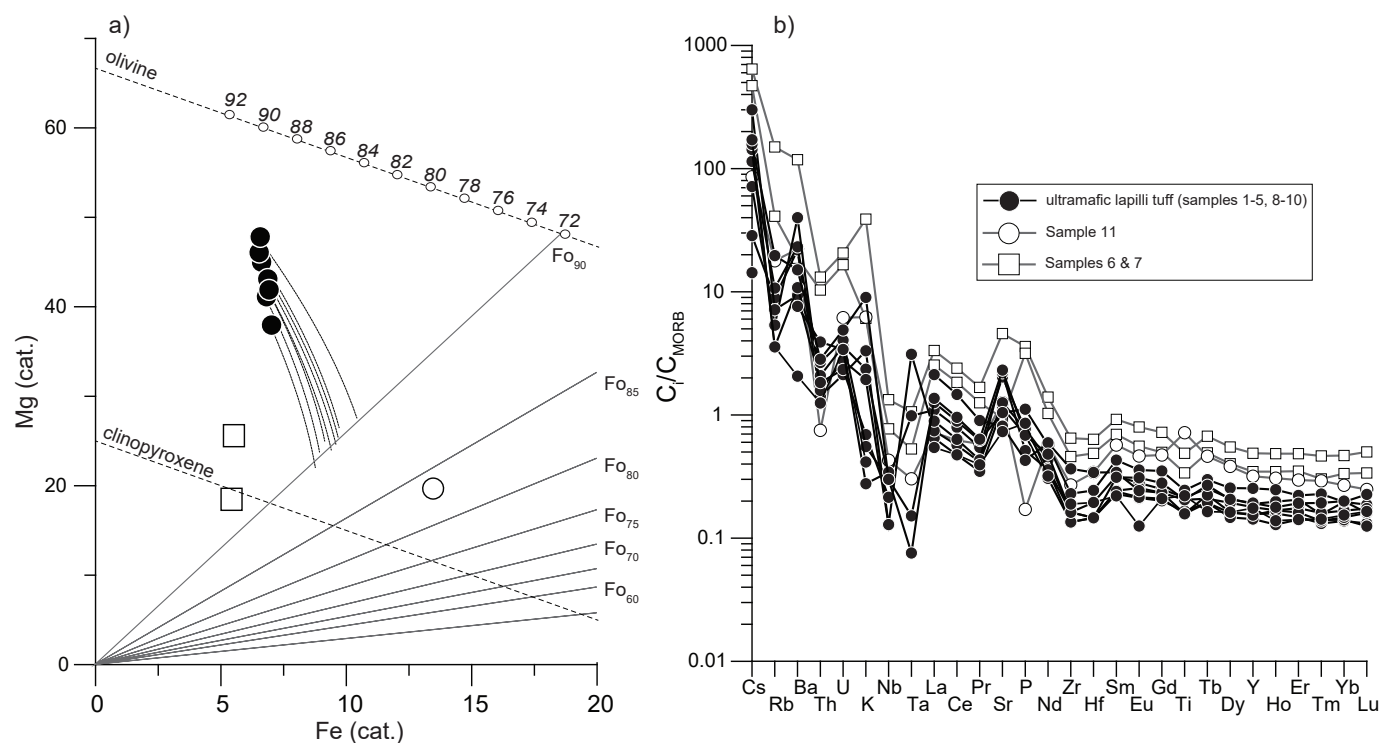


Fig. 8. a) Mg vs. Fe^{TOT} in cation units, showing the compositions of ultramafic lapilli tuff (black circles; samples 1-5, 8-10), olivine clinopyroxenite from Mount Hickman ultramafic complex (white circle; sample 11) and two ultramafic clasts from a basaltic breccia (white squares; samples 6-7). Cation units are calculated by dividing the wt.% oxide value by molecular weight, multiplying by number of cations in oxide formula, and recasting to 100%. The thin dashed lines are the calculated loci of fractional removal of olivine using PRIMELT3 MEGA.XLSM (Herzberg and Asimow, 2015). The radiating lines are isopleths of constant Fo content coexisting with liquids as determined by the Fe-Mg exchange coefficient ($K_D=0.30$) and adjusted for $\text{Fe}^{3+}/\text{Fe}^{\text{TOT}}=0.10$. The stoichiometric compositions of olivine and clinopyroxene are shown for reference. **b)** N-MORB normalized trace element patterns of samples collected during 2009-2011 mapping.

liquid is in equilibrium with Fo_{90} (Herzberg and Asimow, 2015). A relatively low $\text{Fe}^{3+}/\text{Fe}^{\text{TOT}}$ ratio (0.05) was chosen to account for the effect of olivine accumulation, which reduces the $\text{Fe}^{3+}/\text{Fe}^{\text{TOT}}$ ratio of the cumulate rock relative to its parental magma. The calculated primary liquids have high MgO concentrations of 16-20 wt.% (LOI-free), consistent with the paucity of clinopyroxene and plagioclase in the pyroclastic rocks. All of the ultramafic samples are orthopyroxene normative (5-25% by weight). However, because of the high mobility of alkalis and the reduction in Mg/Si ratios that result from conversion of olivine (Mg_2SiO_4) to serpentine ($\text{Mg}_3\text{Si}_2\text{O}_5(\text{OH})_4$), the composition of the parental magma cannot be shown to be subalkaline (Si-saturated) with certainty (Kitayama and Francis, 2014).

The high LOI concentrations and pervasive serpentinization, coupled with the lack of correlation between the mobile (e.g., Ba) and immobile (e.g., Zr) elements (not shown), suggest that LILE contents of the Stuhini Group ultramafic rocks should be considered with caution. In nearly all instances, the absolute abundances of the immobile trace elements are lower than those of mid-ocean ridge basalts (MORB), consistent with dilution by olivine accumulation. The ultramafic rocks have relatively flat MORB-normalized heavy rare earth element (HREE) profiles ($\text{Tb}/\text{Yb}_{\text{MORB}} = 1.1-1.5$), but display relative enrichments in light (L)REE ($\text{Ce}/\text{Yb}_{\text{MORB}} = 3-10$), and marked depletions in high field strength elements (HFSE) relative to

REE of similar compatibility ($\text{Nb}/\text{La}_{\text{MORB}} < 0.3$; $\text{Zr}/\text{Nd}_{\text{MORB}} = 0.3-0.6$).

The single phlogopite-rich olivine clinopyroxenite sample (sample 11, Table 2) from the Mount Hickman ultramafic complex has a relatively high concentration of MgO (~14 wt.%) and CaO (~17 wt.%) and low concentration of Al_2O_3 (~4.5 wt.%), which reflects the predominant control of clinopyroxene accumulation on the sample's chemistry. The sample also contains abundant cumulus magnetite (>10%), which is reflected in its anomalously high Fe content (Fig. 8a). The phlogopite clinopyroxenite sample is depleted in Nb-Ta relative to the similarly compatible LREE, and strongly enriched in LILE, consistent with derivation from a calc-alkaline parental liquid.

The diatreme clasts (6 and 7, Table 2) are picritic (MgO ≥ 16 wt.%) and their strongly altered groundmass accounts for the elevated LOI (4-8 wt.%). In addition to containing ubiquitous clinopyroxene, samples 6 and 7 are distinguished from pyroclastic samples by lower concentrations of MgO and FeO and higher concentrations of Al_2O_3 , TiO_2 , alkalis, and incompatible trace elements. These mineralogical and compositional differences, however, do not preclude a genetic relationship between the clasts and the pyroclastic samples, and future studies may examine possible links.

5. Discussion

5.1. The age of ultramafic volcanism in northern Stikinia

New $^{40}\text{Ar}/^{39}\text{Ar}$ ages from four granodioritic to gabbroic samples indicate that the Hickman pluton cooled through the hornblende closure temperature (400–600°C; Reiners et al., 2005) at ~220–222 Ma, consistent with the previous determination by Holbek (1988). The observation of fresh to partially palagonitized glass in the ultramafic tuff of the Mess Lake facies < 10 km east of the Hickman pluton indicates that the pyroclastic rocks did not experience significant regional metamorphism (Jakobsson and Moore, 1986), suggesting that they may postdate emplacement of the Hickman pluton. This interpretation contradicts that of Logan et al. (2000) who considered the aplitic dikes cutting volcanic rocks of the Mess Lake facies to be co-magmatic with a granodioritic to quartz monzonitic body that they regarded as part of the Hickman pluton farther west (Fig. 2). However, although direct geochronologic data from this eastern plutonic body are lacking, alkaline geochemistry and associated Cu mineralization suggest that its eastern half includes a Late Triassic–Early Jurassic phase belonging to the ca. 195–210 Ma Copper Mountain plutonic suite (Loon Lake stock; cf. Logan et al., 2000). In short, the relative timing of the Mess Lake ultramafic rocks and the Hickman pluton remains unclear. The issue will be addressed by future work including U–Pb (xenocrystic/detrital zircon) and Sm–Nd (whole rock) geochronology of the ultramafic rocks, and $^{40}\text{Ar}/^{39}\text{Ar}$ geochronology of crosscutting hornblende-phyric basaltic dikes (Fig. 3b).

5.2. Emplacement and petrology of the Middle to Upper Triassic ultramafic pyroclastic rocks

The ultramafic pyroclastic rocks of the Mess Lake facies were deposited during at least four cycles of explosive eruption, as recorded by four sharp-based fining-upward sequences. Partially palagonitized, highly-vesicular, scoria (Fig. 6e) and the concavo-convex morphology of bubble-wall glass shards suggest that the ultramafic rocks of the Mess Lake facies were fragmented by violent exsolution of volatiles, rather than by hydrovolcanic explosion (McPhie et al., 1993; Thompson-Stiegler, 2008). We speculate that the lack of epiclastic rocks between each sequence might indicate minimal time gaps between eruptive events.

The calculated MgO contents indicate the Mess Lake facies ultramafic pyroclastic rocks were derived from volatile-rich picritic magmas, undergoing olivine crystallization. The immobile trace element profiles of the pyroclastic rocks resemble many arc-related, calc-alkaline magmatic suites, which are widely regarded as melts of sub-arc asthenosphere metasomatized by fluids ± melts emanating from subducted oceanic lithosphere (Pearce and Peate, 1995). Alternatively, calc-alkaline trace element systematics of the tuffs may be attributed to lithospheric contamination of relatively unfractionated (tholeiitic) parental magmas as commonly proposed for Archean and Proterozoic igneous suites (e.g., Maurice et al., 2009; Milidragovic et al., 2014; Sandeman et

al., 2014). The mass contribution that is required from such a contaminant may be estimated using reservoir-sensitive trace element ratios that are also insensitive to early stages of olivine-predominant fractional crystallization and accumulation (Pearce, 2008). On a Th/Yb vs. Nb/Yb ratio plot (Fig. 9) the ultramafic pyroclastic rocks of the Mess Lake facies plot above the asthenospheric MORB–ocean island basalt (OIB) array. Their position above the array requires either 1) melting of a fluid/melt metasomatized asthenospheric mantle source; or 2) a depleted N-MORB type magma modified by addition of ~10–20% middle and upper crust. Greater amounts of contamination by lower crust would be required to generate the relatively high Th/Yb ratios of the ultramafic pyroclastic rocks. Although this study is in its preliminary stages, we favour the first alternative, in which melting of slab-metasomatized sub-arc asthenosphere is the main control on the trace element profiles of the ultramafic pyroclastics, for three reasons. First, the relatively high volatile contents required for the buoyant ascent of a picritic magma are more consistent with an arc setting. Second, the pseudomorphed olivine crystals are largely euhedral and show no evidence of disequilibrium, which may be expected from assimilation of Si-rich crustal rocks. Third, Pb, which is strongly enriched in the middle and upper crust (15–17 ppm; Rudnick and Gao, 2003) and depleted in N-MORB (0.30 ppm; Sun and McDonough, 1989), is below detection limit (<5 ppm) in all ultramafic samples.

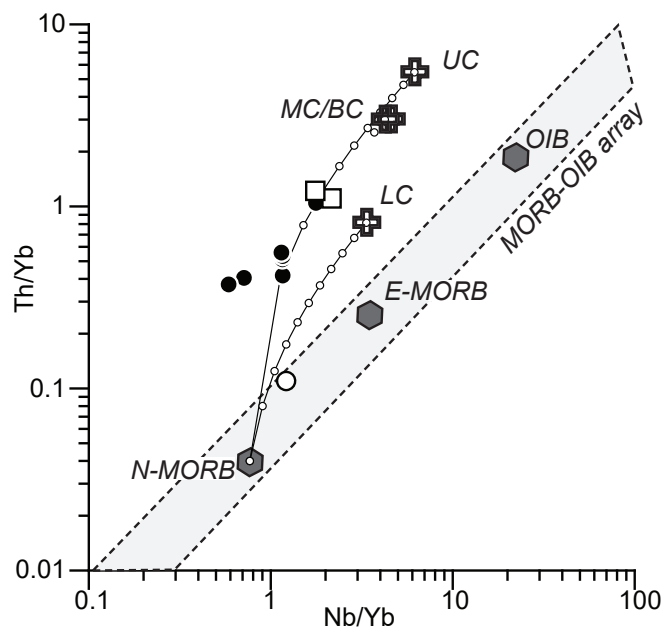


Fig. 9. Th/Yb vs. Nb/Yb (after Pearce, 2008), showing the compositions of ultramafic pyroclastic rocks, olivine clinopyroxenite from the Mount Hickman ultramafic complex, and picritic clasts from a basaltic breccia (symbols as in Fig. 8). The compositions of N-MORB, E-MORB, and OIB are from Pearce (2008); upper continental crust (UC), middle continental crust (MC), lower continental crust (LC) and bulk continental crust (BC) are from Rudnick and Gao (2003). Mixing lines between N-MORB and UC and LC compositions are shown, with small white circles representing 10% mixing steps.

6. Summary and conclusions

Preliminary examination of Middle to Upper Triassic ultramafic volcanic rocks in the Mess Lake area indicates multiple eruptive cycles, evidenced by at least four fining-upward sequences in which sharp-based beds, normally graded from tuff breccia to olivine lapilli tuff, are capped by units of rhythmically stratified ash tuff. Some of the pyroclastic rocks appear to be fresh and contain unaltered glass that is well suited for geochemical studies of magmatic compositions (both major and trace) and volatile contents. Reconstructed primary magma compositions suggest high-MgO (16-20 wt.%) primitive liquids, saturated in olivine only. The ultramafic pyroclastic rocks have typical calc-alkaline trace element signatures (Pearce and Peate, 1995), consistent with derivation from metasomatized, sub-arc asthenospheric mantle. Future studies will examine possible genetic links between the pyroclastic deposits, mafic-ultramafic cumulate intrusions of the Polaris Suite, and diatreme(s) containing picritic clasts.

Fresh volcanic glass in the ultramafic tuffs adjacent to the Hickman pluton and diatreme(s) cutting the Hickman pluton support the idea that ultramafic volcanism, as a whole, is younger than the hornblende age of the Hickman pluton (~222 to 220 Ma). This is at odds with the observations of Logan et al. (2000), who reported that aplitic dikes emanating from a hornblende granodioritic to quartz monzonitic body, which they considered correlative with the Hickman pluton, cut volcanic rocks of the Mess Lake facies. Uranium-lead, $^{40}\text{Ar}/^{39}\text{Ar}$, and Sm-Nd geochronology will be used to better constrain the emplacement age of the ultramafic rocks, and isotopic studies (Rb-Sr and Sm-Nd) will be used to assess the contributions of different reservoirs during ultramafic magma petrogenesis and, ultimately, to help further characterize mantle conditions during the deposition of the Stuhini Group and spatially associated ultramafic plutons.

Acknowledgments

The project is funded by the Geological Survey of Canada's Geomapping for Energy and Minerals program (GSC contribution #2015-0348), with logistical support from Teck Resources. We especially thank Klaus Hepe, Gabe Jutras, and Leif Bailey (Teck) for facilitating our fieldwork out of the Schaft Creek exploration camp. Sebastian Bichlmaier and Simon Carroll provided superb assistance in the field. The manuscript benefited from the attentive reviews by L. Ootes and L. Aspler.

References cited

- Barresi, T., Nelson, J.L., Dostal, J., and Friedman, R., 2015. Evolution of the Hazelton arc near Terrace, British Columbia: stratigraphic, geochronological, and geochemical constraints on a Late Triassic-Early Jurassic arc and Cu-Au belt. *Canadian Journal of Earth Sciences*, 52, 466-494.
- British Columbia Geological Survey, 2015. MINFILE—British Columbia mineral deposits database. British Columbia Ministry of Energy and Mines, <http://minfile.gov.bc.ca/>.
- Brown, D.A., Gunning, M.H., and Greig, C.J., 1996. The Stikine project: geology of the western Telegraph Creek map area, Northwestern British Columbia (NTS 104G/5, 6, 11W, 12 and 13). British Columbia Ministry of Energy, Mines and Natural Gas, British Columbia Geological Survey Bulletin 95, 175 p.
- Herzberg, C. and Asimow, P.D., 2015. PRIMELT3 MEGA. XLSM software for primary magma calculation: peridotite primary magma MgO contents from the liquidus to the solidus. *Geochemistry, Geophysics, Geosystems*, 16, 16 p.
- Holbek, P.M., 1988. Geology and mineralization of the Stikine Assemblage, Mess Creek Area, northwestern British Columbia. Unpublished M.Sc. thesis, The University of British Columbia, 184 p.
- Jakobsson, S. P. and Moore, J.G., 1986. Hydrothermal minerals and alteration rates at Surtsey volcano, Iceland. *Geological Society of America Bulletin*, 97, 648-659.
- Kellett, D. and Joyce, N., 2014. Analytical details of the single- and multicollection $^{40}\text{Ar}/^{39}\text{Ar}$ measurements for conventional step-heating and total-fusion age calculation using the Nu Noblesse at the Geological Survey of Canada. Geological Survey of Canada, Technical Note 8, 27 p.
- Kitayama, Y. and Francis, D., 2014. Iron-rich alkaline magmatism in the Archean Wawa greenstone belts (Ontario, Canada). *Precambrian Research*, 252, 53-70.
- Koppers, A.A.P. 2002. ArArCALC – software for $^{40}\text{Ar}/^{39}\text{Ar}$ age calculations. *Computers and Geosciences*, 28, 605-619.
- Kuiper, K. F., A. Deino, F. J. Hilgen, W. Krijgsman, P. R. Renne and J. R. Wijbrans, 2008. Synchronizing rock clocks of Earth history. *Science*, 320, 500-504.
- Logan, J.M. and Koyanagi, V.M., 1994. Geology and mineral deposits of the Galore Creek area, northwestern British Columbia (104G/3 and 4). British Columbia Ministry of Energy, Mines and Petroleum Resources, British Columbia Geological Survey Bulletin 92, 96 p.
- Logan, J.M. and Iverson, O., 2013. Dease Lake geoscience project: geochemical characteristics of Tsaybahe, Stuhini, and Hazelton volcanic rocks, northwestern British Columbia (NTS 104I, J). In: *Geoscience BC Summary of Activities 2012*, Geoscience BC, Report 2013-1, pp. 11-32.
- Logan, J.M. and Mihalynuk, M.G., 2014. Tectonic controls on early Mesozoic paired alkaline porphyry deposit belts (Cu-Au ±Ag-Pt-Pd-Mo) within the Canadian Cordillera. *Economic Geology*, 109, 827-858.
- Logan, J.M., Drobe, J.R., and McClelland, W.C., 2000. Geology of the Forrest Kerr-Mess Creek Area, Northwestern British Columbia (NTS 104B/10, 15 & 104/G2 & 7W). British Columbia Ministry of Energy, Mines and Petroleum Resources, British Columbia Geological Survey Bulletin 104, 164 p.
- Maurice, C., David, J., Bedard, J.H, and Francis, D., 2009. Evidence for a widespread mafic cover sequence and its implications for continental growth in the Northeastern Superior Province. *Precambrian Research*, 168, 45-65.
- McPhie, J., Doyle, M., and Allen, R., 1993. Volcanic textures: A guide to the interpretation of textures in volcanic rocks. ARC Centre of Excellence in Ore Deposits, University of Tasmania, 190 p.
- Milidragovic, D., Francis, D., Weis, D., and Constantin, M., 2014. Neoproterozoic (c. 2.7 Ga) plutons of the Ungava craton, Quebec, Canada: parental magma compositions and implications for Fe-rich mantle source regions. *Journal of Petrology*, 55, 2481-2512.
- Mihalynuk, M.G., Bellefontaine, K.A., Brown, D.A., Logan, J.M., Nelson, J.L., Legun, A.S. and Diakow, L.J., 1996. Geological compilation, northwest British Columbia (NTS 94E, L, M; 104F, G, H, I, J, K, L, M, N, O, P; 114J, O, P). BC Ministry of Energy and Mines, British Columbia Geological Survey Open File 1996-11.
- Mihalynuk, M.G., Mountjoy, K.J., Smith, M.T., Currie, L.D., Gabites, J.E., Tipper, H.W., Orchard, M.J., Poulton, T.P., and Cordey, F., 1999. Geology and mineral resources of the Tagish

- Lake area (NTS 104M/ 8,9,10E, 15 and 104N/ 12W), northwestern British Columbia. British Columbia Ministry of Energy and Mines, British Columbia Geological Survey Bulletin 105, p. 217.
- Min, K., Mundil, R., Renne, P.R., Ludwig, K.R., 2000. A test for systematic errors in $^{40}\text{Ar}/^{39}\text{Ar}$ geochronology through comparison with U/Pb analysis of a 1.1 Ga rhyolite. *Geochimica Cosmochimica Acta*, 64, 73-98.
- Monger, J.W.H., 1977. Upper Paleozoic rocks of the western Canadian Cordillera and their bearing on Cordilleran evolution. *Canadian Journal of Earth Sciences*, 14, 1832-1859.
- Nelson, J., Colpron, M., and Israel, S., 2013. The Cordillera of British Columbia, Yukon and Alaska: tectonics and metallogeny. In: Colpron, M., Bissig, T., Rusk, B., and Thompson, J.F.H., (Eds.), *Tectonics, Metallogeny, and Discovery - the North American Cordillera and similar accretionary settings*. Society of Economic Geologists, Special Publication 17, pp. 53-109.
- Nixon, G.T., Ash, C.H., Connely, J.N., and Case, G., 1989. Alaskan-type mafic-ultramafic rocks in British Columbia: the Gnat Lakes, Hickman, and Menard Creek complexes. In: *Geological Fieldwork 1988*, British Columbia Ministry of Energy, Mines and Petroleum Resources, British Columbia Geological Survey Paper 1989-1, pp. 429-442.
- Pearce, J.A., 2008. Geochemical fingerprinting of oceanic basalts with applications to ophiolite classification and the search for Archean oceanic crust. *Lithos*, 100, 14-48.
- Pearce, J.A. and Peate, D.W., 1995. Tectonic implications of the composition of volcanic arc magmas. *Annual Reviews of Earth and Planetary Sciences*, 23, 251-285.
- Reiners P.W., Ehlers, T.A., and Zeitler, P.K., 2005. Past, present, and future of thermochronology. *Reviews in Mineralogy and Geochemistry*, 58, 1-18.
- Richards, J.P., 2015. The oxidation state, and sulfur and Cu contents of arc magmas: implications for metallogeny. *Lithos*, 233, 27-45.
- Roddick, J. C., Cliff, R. A., and Rex, D. C, 1980. The evolution of excess argon in alpine biotites, *Earth and Planetary Science Letters*, 48, 185-208.
- Roddick, J.C., 1988. The assessment of errors in $^{40}\text{Ar}/^{39}\text{Ar}$ dating. In: *Radiogenic Age and Isotopic Studies, Report 2*. Geological Survey of Canada, Paper 88-2, pp. 7-16.
- Roddick, J.C., Cliff, R.A., and Rex, D.C., 1980. The evolution of excess argon in alpine biotites - a $^{40}\text{Ar}/^{39}\text{Ar}$ analysis. *Earth and Planetary Science Letters*, 48, 185-208.
- Rudnick, R.L. and Gao, S., Composition of the continental crust. In: Holland, H.D, Turekian, K.K. (Eds.), *Treatise on Geochemistry*. Rudnick, R.L. (E.D), *The Crust*, vol. 3, Elsevier-Pergamon, Oxford, pp. 1-64.
- Sandeman, H.A., Ootes, L., Cousens, B., and Killian, T., 2014. Petrogenesis of Gunbarrel magmatic rocks: homogeneous continental tholeiites associated with extension and rifting of Neoproterozoic Laurentia. *Precambrian Research*, 252, 166-179.
- Scaillet, S., 2000. Numerical error analysis in $^{40}\text{Ar}/^{39}\text{Ar}$ dating, *Chemical Geology*, 162, 269-298.
- Sun, S. and McDonough, W., 1989. Chemical and isotopic systematics of oceanic basalts: implications for mantle composition and processes. In: Saunders, A.D and Norry, M.J (Eds.) *Magmatism in the Ocean Basins*, Geological Society of London Special Publication 42, pp. 313-435.
- Souther, J.G., 1977. Volcanism and tectonic environments in the Canadian Cordillera – A second look. In: Baragar, W. R.A., Coleman, L.C., and Hall, J.M., (Eds.) *Volcanic Regimes of Canada*. Geological Association of Canada Special Paper 16, pp. 1-24.
- Thompson Stiegler, M. Lowe, R., and Byerly, G.R., 2008. Abundant pyroclastic komatiitic volcanism in the 3.5-3.2 Ga Barberton greenstone belt, South Africa. *Geology*, 36, 779-782.
- Yukon Geological Survey, 2015. Yukon MINFILE mineral occurrences and deposits database: Yukon Energy, Mines and Resources, <http://ygsftp.gov.yk.ca/httpdocs/minfile/index.html>.
- Zagorevski, A., Mihalynuk, M.G., Joyce, N., and Martin, K., 2014. Characterization of volcanic and intrusive rocks across the British Columbia-Yukon border, GEM 2 Cordillera. Geological Survey of Canada, Open File 7697, 10 p.

